



HAL
open science

Evaluating ice-rafted debris as a proxy for glacier calving in Upernavik Isfjord, NW Greenland

Flor Vermassen, David Wangner, Laurence M Dyke, Sabine Schmidt, Amalie Cordua, Kurt Kjær, Konstanze Haubner, Camilla S Andresen

► **To cite this version:**

Flor Vermassen, David Wangner, Laurence M Dyke, Sabine Schmidt, Amalie Cordua, et al.. Evaluating ice-rafted debris as a proxy for glacier calving in Upernavik Isfjord, NW Greenland. *Journal of Quaternary Science*, 2019, 34 (3), pp.258-267. 10.1002/jqs.3095 . hal-02357292

HAL Id: hal-02357292

<https://hal.science/hal-02357292>

Submitted on 31 Aug 2021

HAL is a multi-disciplinary open access archive for the deposit and dissemination of scientific research documents, whether they are published or not. The documents may come from teaching and research institutions in France or abroad, or from public or private research centers.

L'archive ouverte pluridisciplinaire **HAL**, est destinée au dépôt et à la diffusion de documents scientifiques de niveau recherche, publiés ou non, émanant des établissements d'enseignement et de recherche français ou étrangers, des laboratoires publics ou privés.



Distributed under a Creative Commons Attribution - NonCommercial - NoDerivatives 4.0 International License

Evaluating ice-rafted debris as a proxy for glacier calving in Upernavik Isfjord, NW Greenland

FLOR VERMASSEN,^{1,2*} DAVID J. WANGNER,^{1,2} LAURENCE M. DYKE,¹ SABINE SCHMIDT,³ AMALIE E. CORDUA,⁴ KURT H. KJÆR,² KONSTANZE HAUBNER^{1,2} and CAMILLA S. ANDRESEN¹

¹Geological Survey of Denmark and Greenland, Department of Glaciology and Climate, Copenhagen, Denmark

²Centre for GeoGenetics, Natural History Museum of Denmark, University of Copenhagen, Copenhagen, Denmark

³CNRS, OASU, EPOC, UMR5805, Pessac Cedex, France

⁴Institute for geology, University of Hamburg, Hamburg, Germany

Received 14 March 2018; Revised 7 February 2019; Accepted 7 February 2019

ABSTRACT: Records of ice-rafted debris (IRD) in sediments are commonly used as a proxy for iceberg production and to reconstruct past changes of glacier stability. However, the interpretation of IRD is complex as multiple processes modulate its variability. This study investigates the relationship between IRD variability and glaciological change by measuring IRD records from Upernavik Fjord and comparing these to frontal positions of Upernavik Isstrøm during the past century. Results show that the spatial variability of IRD deposition throughout the fjord is high, indicating that randomness inherent to IRD distorts the calving signal. However, we investigate whether IRD records can be combined to improve the reconstruction, as previously suggested, and show the importance of core site selection and number of cores on this approach. The outer-fjord core compares relatively well to the observed front positions and this is reflected in the composite record: increased IRD deposition in 1937–1946, 1968–1980, and 1996–1999 occurred during periods of faster retreat. Comparison with climatic records shows that the calving episodes in the late '30s/early '40s and late '90s are related to warm ocean and air temperatures, whereas intensified retreat and calving during the '70s reflects partly an internal glacier response to the fjord geometry. © 2019 The Authors. *Journal of Quaternary Science* Published by John Wiley & Sons Ltd.

KEYWORDS: glacier retreat; ice-rafted debris; proxy evaluation; Upernavik Isfjord; Upernavik Isstrøm

Introduction

The sudden increase in mass loss from the Greenland Ice Sheet at the onset of this century has spurred investigations regarding ice-discharge at marine terminating glaciers, a process that contributes up to 50% of Greenland's total ice mass loss (Straneo and Heimbach, 2013; van den Broeke et al., 2016). In order to improve sea-level projections a better understanding of glacier dynamics over decadal, centennial, and millennial timescales is required. In palaeoceanographic research, past glacier or ice sheet activity is frequently reconstructed by quantifying the amount of ice-rafted debris (IRD) in sediment cores (Andrews, 2000; Kuijpers et al., 2014). IRD is a terrigenous material transported within a matrix of ice and deposited in marine (or lacustrine) sediments when the ice matrix melts (Kuijpers et al., 2014). Multiple ways to quantify IRD exist, one of these is to measure the weight percentage of sand-sized sediment. This is done under the assumption that these grains are too coarse to be deposited by any other sedimentation process. The IRD proxy has traditionally been used to identify Heinrich layers in the North-Atlantic; rapidly deposited layers of IRD that attest to episodes of abrupt climate change during past glacial cycles (Andrews, 2000; Heinrich, 1988; Kuijpers et al., 2014). More recently, Andresen et al. (2011) have measured down-core variations in IRD in sediment from Sermilik Fjord and showed a correspondence with the observed 20th and 21st century glacier front positions of Helheim glacier, thereby relating the IRD signal to the calving intensity of the glacier.

Although the use of IRD as a proxy for glaciological change is common practice, interpretation of IRD records can be complicated due to multiple glaciological, climatological, and sedimentological factors (Andrews, 2000). A better under-

standing of these complexities can be achieved by comparing IRD records to direct observations of glacier change. Glaciated fjords in Greenland can provide ideal conditions for such studies as relatively rapid sedimentation rates permit the reconstruction of IRD with a high temporal resolution (i.e. decadal/annual). In addition, a few sites around Greenland benefit from historical documentation of past glacier margin positions, extending records of glacier change back to the 19th Century. Another advantage of investigating IRD records in fjords is that the iceberg source is well-defined and does not suffer from uncertainties regarding variable source input from distal glaciers (or ice sheets). In this study, sediment cores from a fjord transect are investigated for their IRD content and assessed against glacier margin changes of Upernavik Isstrøm (UI) and climate records in order to gain a better understanding of IRD variability and its interpretation.

Upernavik Isfjord and Isstrøm

Upernavik Isstrøm consists of four major marine terminating outlet glaciers with a combined catchment area of 64,667 km² (Haubner et al., 2017). In 1886 the ice stream was characterised by a single glacier front, but it has subsequently retreated into different branches of the fjord, creating the four glaciers that currently calve into the fjord (Upernavik 1–4, Fig. 1) (Andresen et al., 2014; Weidick, 1958). The split-up between a northern and southern branch occurred in the late '30s. The southern branch decoupled again after 1949, creating Upernavik 3 and 4 (UI-3, UI-4). The northern branch decoupled after 1966, thereby forming Upernavik 1 and 2 (UI-1, UI-2).

Upernavik Isfjord has a length of ~60 km and is 5–7 km wide. The fjord floor has been mapped with a Multibeam Echo Sounder System as part of NASA's Oceans Melting Greenland

*Correspondence: Flor Vermassen, Geological Survey of Denmark and Greenland, Department of Glaciology and Climate, Copenhagen, Denmark. E-mail: flv@geus.dk

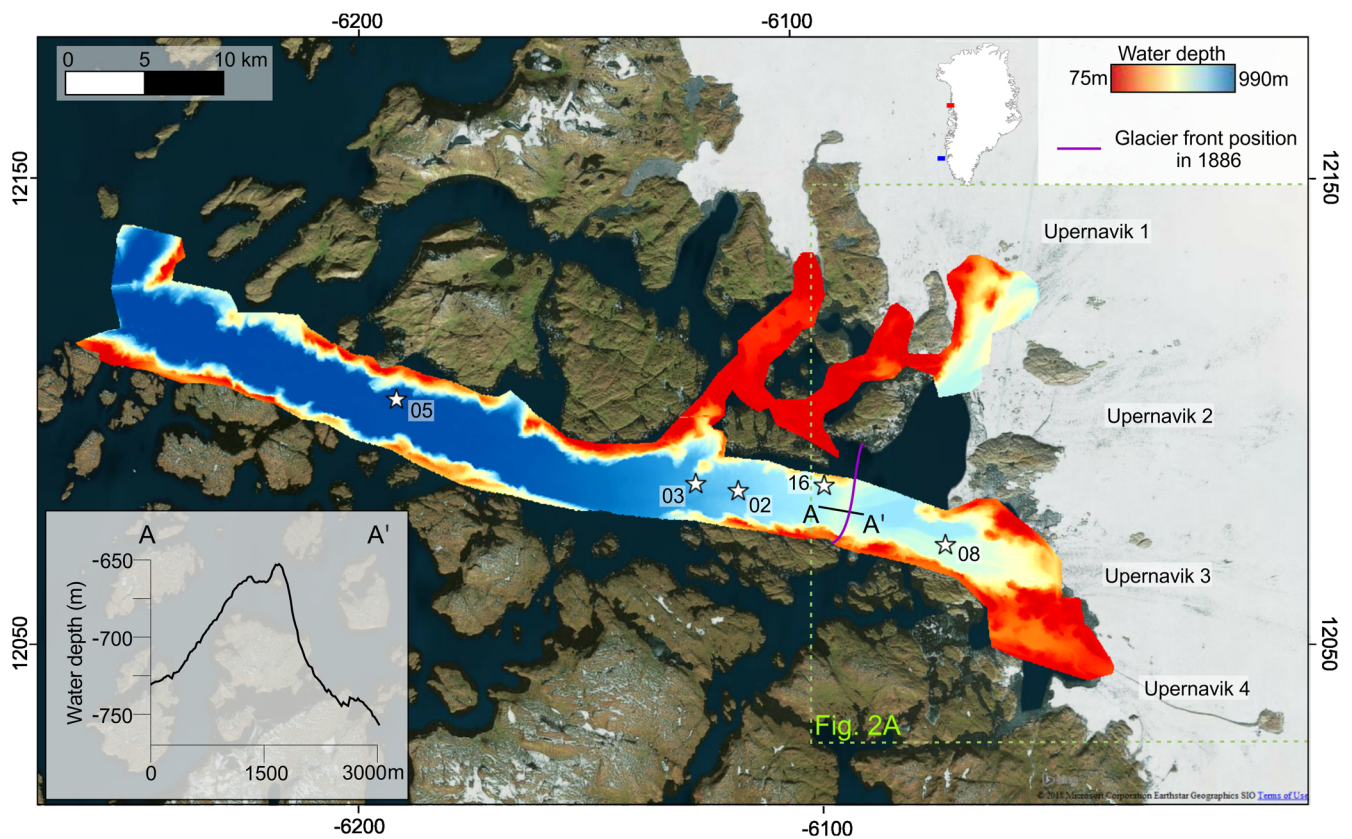


Figure 1. Bathymetry and surroundings of Upernavik Isfjord, West Greenland, together with the locations of the cores investigated in this study. The bathymetry is from the NASA OMG mission (NASA, 2016). The location of Fig. 2A is indicated by the green dashed line. The inset show a cross-profile of a bathymetric high present in the fjord. The projection used is WGS84/Pseudo-Mercator (EPSG:3857). [Color figure can be viewed at wileyonlinelibrary.com]

mission (NASA OMG Mission, 2016). The outer-fjord is characterised by steep sided walls and a flat, largely featureless fjord floor at ~900 m water depth. A bathymetric high rises 150 m above the surrounding fjord floor where the glacier front was positioned in 1886 (Fig. 1). This feature is orientated perpendicular to the fjord axis (Fig. 1). The southern branch of the fjord is relatively shallow (i.e. where UI-3 and UI-4 terminate) (70–500 m, Fig. 1). In contrast, the northern branch (i.e. where UI-3 and UI-4 terminate) remains deep to the glacier calving front (~700 m, Fig. 1).

Recent CTD measurements have revealed a stratified water column in Upernavik Isfjord with evidence for warm water entrainment near the glacier front (Fenty *et al.*, 2016), this is typical of large, deep glaciated fjords around Greenland (Straneo and Heimbach, 2013). The stratification is the result of the different ocean currents that influence the hydrography of the fjord. The deeper layer is derived from the North Atlantic Current and has a subtropical origin. This water mass is delivered to Upernavik Fjord by the West Greenland Current, a boundary current which becomes progressively cooler and fresher as it flows northward along the West Greenland shelf (Ribergaard *et al.*, 2008). The cold upper layer originates in the Arctic Ocean and is augmented by glacial meltwater. The bedrock surrounding UI consists primarily of Precambrian charnockite, an orthopyroxene-bearing granite that forms part of the Prøven igneous complex (Escher and Pulvertaft, 1995).

Methods

Core collection and sub-sampling

The five sediment cores investigated in this study (1.2–1.7 m core length) were collected in August 2013 onboard R/V Porsild along a fjord-axis transect in water depths between 680

and 1000 m (Fig. 1). Coring was undertaken with a Rumohr corer (Meischner and Rumohr, 1974). This type of device is specifically designed to avoid sediment disturbance during coring, thereby aiming to preserve the core top. All cores were sampled continuously at 1 cm resolution for grain size analysis. Water content was calculated by weighing sediment samples before and after freeze-drying.

X-ray imaging

X-ray imaging of the sediment cores after splitting was performed at the Danish National Museum, Department of Conservation (Brede, DK). Imaging was performed with the YXLON Smart 160E/0.4 X-ray unit. It was operated at 3 mA and 90 kV, with an exposure time of 120 seconds. The X-rays were detected on phosphor plates with a 0.5 mm iron filter, placed 105 cm from the source. Subsequently, the radiographs were digitalised with a Duerr HD-CR 35 NDT scanner, with a scan line width of 50 μm . The full-core radiographs presented in this paper were compiled from individual radiographs that each span around 50 cm of core length. The relatively large X-ray step-size results in a subtle artefact (horizontal line) at the image boundaries; this occurs approximately every 50 cm in the compiled images.

Grain-size analysis

Wet-sieving was performed on all samples, separating them into three grain-size fractions (<63 μm , 63–125 μm , and >125 μm). The different fractions were weighed and the individual percentages were calculated relative to the total dry weight. For the >125 μm fraction, individual grains that weighed more than 0.01 g were discarded in order to reduce distortion of the grain size signal resulting from the occurrence of large grains.

By assuming these grains have a granitic composition (2.7 g cm^{-3}) and a spherical shape, the weight limit of 0.01 g was converted to a grain-size limit of 4 mm diameter.

Ice-rafted debris in marine sediment cores is usually quantified by measuring the weight percentage of a certain coarse size fraction (Kuijpers *et al.*, 2014). However, the temporal variability in weight percentage of a coarse fraction does not provide an unequivocal indication of variability in iceberg rafting since the weight percentage data do not take into account the sedimentation rate (the time allowed to deposit the iceberg rafted sediment). Consequently, the percentage data of the coarse size fractions is converted to the absolute flux of coarse material to the fjord floor ($\text{g cm}^{-3} \text{ a}^{-1}$). In this study this conversion does not change the relative variability considerably because changes in water content are minimal and the CF-CS model assumes a constant sedimentation rate. Nevertheless, the calculation of IRD flux offers the advantage that these numbers can be compared between cores (and other studies) and allow the calculation of averaged IRD fluxes (Andresen *et al.*, 2012). The IRD flux is calculated with the formula:

$$F = \frac{S}{W} \times P \times d$$

With

F = IRD flux [$\text{kg/m}^2 \times \text{yr}$]

S = Sedimentation rate [m/yr]

W = Water content (%)

P = Weight percentage of the $63\text{--}4000 \mu\text{m}$ fraction (%)

d = Grain density (quartz) [2.7 kg/m^3]

Core chronology

Age constraint of the sediments was achieved through ^{210}Pb dating. A one cm thick slice of core material was sampled at 5 cm intervals from the surface of the core to a depth of 20 cm , and at 10 cm intervals below this. After drying, $4\text{--}6 \text{ g}$ of each

sediment sample was conditioned in sealed vials. Measurements of ^{210}Pb , ^{226}Ra and ^{137}Cs activities were performed using a well-type gamma detector Cryocycle-I (Canberra) at the laboratory UMR5805 EPOC (University of Bordeaux, France). Estimated errors of radionuclide activities are based on 1 standard deviation counting statistics. Excess ^{210}Pb ($^{210}\text{Pb}_{\text{xs}}$) is calculated by subtracting the activity supported by its parent isotope, ^{226}Ra , from the total ^{210}Pb activity in the sediment. The CF-CS (constant flux, constant sedimentation) model was applied to calculate a maximum sedimentation rate. These sedimentation rates were used to calculate sediment ages. This approach assumes that the sediment surface represents the year of core acquisition (2013).

The artificial radioisotope ^{137}Cs is often used as an independent time marker in order to validate the ^{210}Pb age model. The onset of ^{137}Cs in marine sediments occurred in the early '50s. Sedimentary ^{137}Cs profiles usually exhibit a peak in 1963 related to the maximum fallout from atmospheric nuclear weapon tests in the Northern Hemisphere (Appleby, 2008; MacKenzie *et al.*, 2011). Sediments may also exhibit a smaller, younger peak which corresponds to ^{137}Cs released during the 1986 Chernobyl nuclear accident (Klouch *et al.*, 2016).

Calculation of area change

Glacier frontal positions were derived from historical observations compiled by Weidick (1958), and from aerial and satellite imagery (Andresen *et al.*, 2014; Khan *et al.*, 2013) (Fig. 2). We calculate the glacier area change through time from these data by digitising glacier frontal positions using the geospatial software QGIS 2.18 (Fig. 2, data available in Table S1).

Results

Sedimentary facies and stratigraphy

Sediments within Upernavik Isfjord are divided into three lithofacies: diamicton, gravity flow deposits, and homogeneous

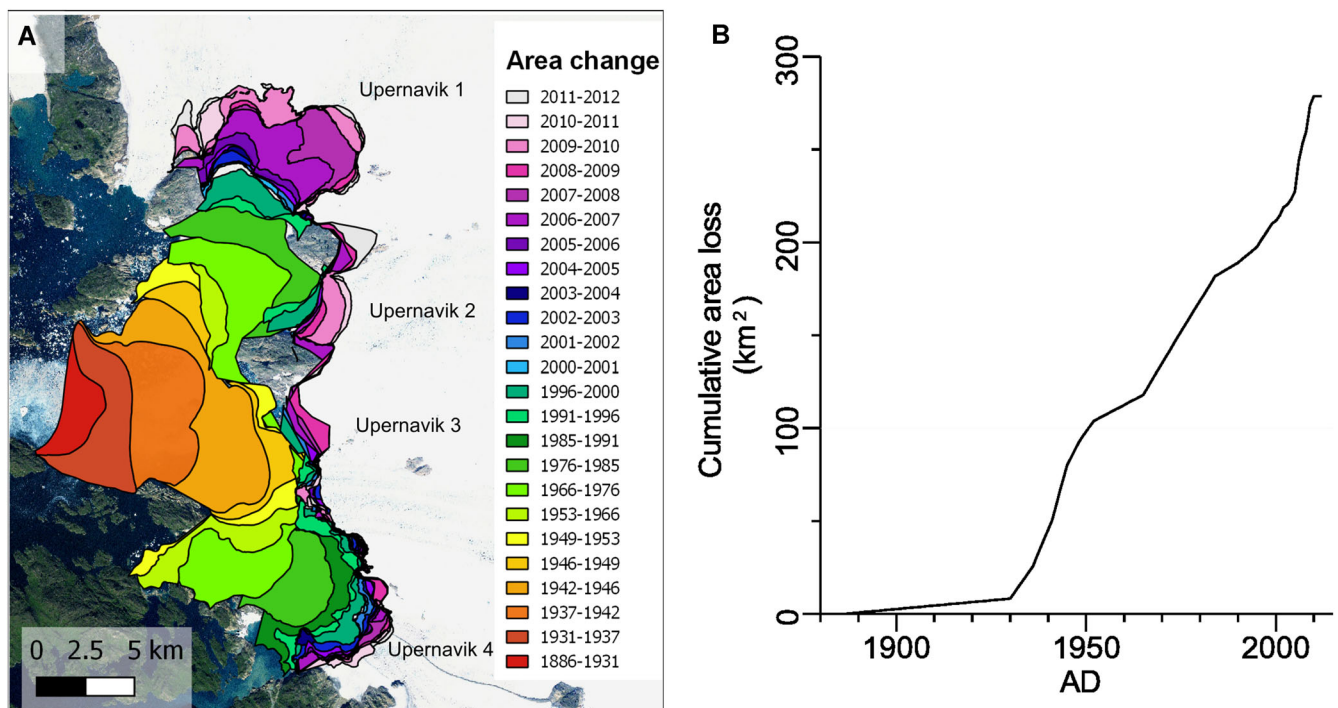


Figure 2. A) Calculation of glacier area change of UI since 1886, derived from a combination of visual observations and satellite imagery (Andresen *et al.*, 2014; Khan *et al.*, 2013; Weidick, 1958). B) Total cumulative area loss of UI between 1886 and 2012 (Table S1). [Color figure can be viewed at wileyonlinelibrary.com]

mud. (Fig. 3). These facies are defined on the basis of linescans, X-ray imagery, and visual core description. The diamicton unit is composed of outsized clasts that are interspersed in a mud matrix. The coarse clasts are poorly-sorted and matrix-supported; this is typical of ice-rafted debris. Ice-rafting in glacimarine fjords is a primary sedimentation process, and diamicton is often interpreted as formed by a combination of ice-rafting and settling of fines from meltwater plumes (Dowdeswell *et al.*, 1994). The diamicton is further divided into three subfacies (Fig. 3): massive, stratified, and coarse

diamicton. The coarser diamicton is composed primarily of coarse sand and gravel. The clasts are grain-supported with limited (fine) matrix. This facies occurs in distinct layers characterised by a well-defined lower boundary and a subtle fining-upwards trend. This facies probably represents rapid sediment deposition events related to iceberg-rafting. For example, the dumping of sediment during iceberg turnover, sudden iceberg collapse and melt, or the rapid local melt-out of coarse basal debris. Gravity flow deposits are characterised by a well-sorted layer of sand that generally fine upwards and


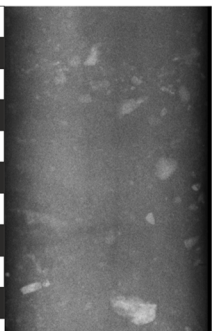
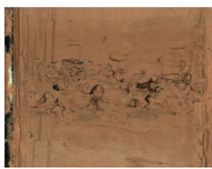
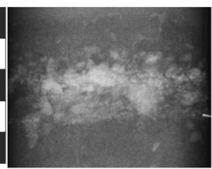

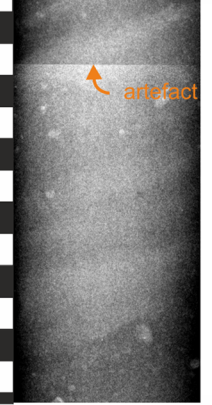



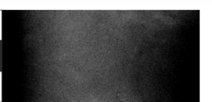
Lithofacies Subfacies	Lithofacies description	Core surface linescan	X-Radiograph
Diamicton	Massive		
	coarse		
	Laminated		
	Gravity flow deposit		
	Homogeneous mud		

Figure 3. Description of the sedimentary facies, illustrated by the linescan and x-radiograph. Bar segments are 1 cm. [Color figure can be viewed at wileyonlinelibrary.com]

have a sharp lower boundary, these occasionally occur in stacked sequences. We interpret these deposits as fine-grained turbidites (Bouma, 1962). Homogeneous mud is characterised by fine sediments that contain no outsized clasts. Grain-size data is available in Tables S2–S6.

POR13-03, -02, and -16 are predominantly composed of either massive or subtly stratified diamicton (Fig. 4), these are sporadically interrupted by thin turbidites. These occur below the levels for which the age models were developed, and thus do not interfere with the IRD records presented here. Layers of coarser diamicton are present in cores POR13-03 (72–77 and 88–92 cm) and POR13-16 (77–80 cm). POR13-05 has the most varied lithology. The lower part of the core (90–172 cm) is characterised by alternating layers of diamicton and homogeneous mud with little or no IRD. The mid-section of the core contains a thick turbidite (70–90 cm). The upper-part of the core (0–70 cm) is composed of massive diamicton.

Age models

The ^{210}Pb -based dating method relies on the occurrence of unsupported lead. In all five cores $^{210}\text{Pb}_{\text{xs}}$ decreases with depth in a logarithmic trend (Fig. 5, data available in Table S7). The age models are restricted to the maximum depth to which unsupported ^{210}Pb could be measured ($>3 \text{ mBq g}^{-1}$). In cores POR13-02, -05, and -16 $^{210}\text{Pb}_{\text{xs}}$ was detected in the uppermost 50 cm. In core POR13-03, the occurrence of significant, although low, $^{210}\text{Pb}_{\text{xs}}$ is limited to the upper 11 cm (Fig. 5), the activities measured below (13, 17, and 20 cm) are almost equal to ^{226}Ra . Although the low levels of ^{137}Cs preclude the identification of peaks, the presence of detectable ^{137}Cs indicates that these sediments are younger than 1950, this is consistent with the age models (Fig. S1, Table S7).

Sedimentation rates in Upernavik Isfjord vary between 0.4 and 1.2 cm a^{-1} . These relatively high rates are typical for glacial fjords, as sediment is mainly delivered by melt-water plume deposition and iceberg-rafting (Ó Cofaigh and Dowdeswell, 2001).

Grain-size analysis and ice-rafted debris

Sediments from Upernavik Isfjord are predominantly fine-grained; silt and clay make up 93–97% of the cores by weight (Fig. 4). The 63–125 μm fraction generally constitutes 1–2% of the sediment and the 125–4000 μm fraction about 1–5%.

The 125–4000 μm fraction displays a higher frequency of variability relative to the 63–125 μm fraction (Fig. 6, Tables S2–S6).

The largest discrepancies between the coarse fractions occur in levels dominated by turbidites. Thin turbidites are typically well-sorted and consequently they are observed as a prominent peak in one specific grain size fraction (e.g. POR13-03, 49–50 cm; POR13-16, 78–80 cm, Fig. 4).

The two fractions (63–125 μm and 125–4000 μm) were measured to investigate whether the choice of grain-size fraction influences the recorded IRD signal (Fig. 6, Tables S2–S6). In core POR13-05 the two sand-size fractions are well correlated (correlation coefficient = 0.79, Fig. 5). For cores POR13-03 and -16, the correlation is lower ($r = 0.57$ and 0.51, respectively). Core POR13-16 exhibits a low correlation between the two fractions ($r = 0.30$). Generally, these results show that, within one core, the two grain-size fractions are characterised by similar timing of peaks, but that the relative amplitude of those peaks can vary between size fractions. Consequently, care should be taken in comparing the amplitude of IRD peaks of narrow fractions in the sand and clast size, when evaluating temporal variability in iceberg rafting. Therefore we use the broad 63–4000 μm fraction here.

Discussion

IRD variability in Upernavik Isfjord

Environmental factors such as sea-ice conditions (frozen vs. unfrozen fjord) and ambient water temperature can depress or enhance the general ice-rafting signal and therefore complicate its interpretation as an indicator of calving intensity. In addition, IRD variability has an inherent random component due to local effects such as differential iceberg transport pathways and variations in the sediment load and grain-size distribution of icebergs (Andrews, 2000; Wangner *et al.*, 2018). Our results confirm this high spatial variability since the IRD fluxes vary markedly between core sites with little to no correlation (Fig. 7). By comparing these results to a record of glacier front positions we are able to investigate the relationship between IRD and glaciological change better. This evaluation relies on the fact that periods of front retreat are expected to coincide with an increased calving rate, since calving is the dominant processes of frontal ablation of tidewater glaciers. Still, some differences may occur because front position is the result of ice supply vs. frontal ablation, and increased ice supply can compensate increased calving rates (and vice versa). Nevertheless, it can be expected that multi-year periods of retreat broadly correspond with increased

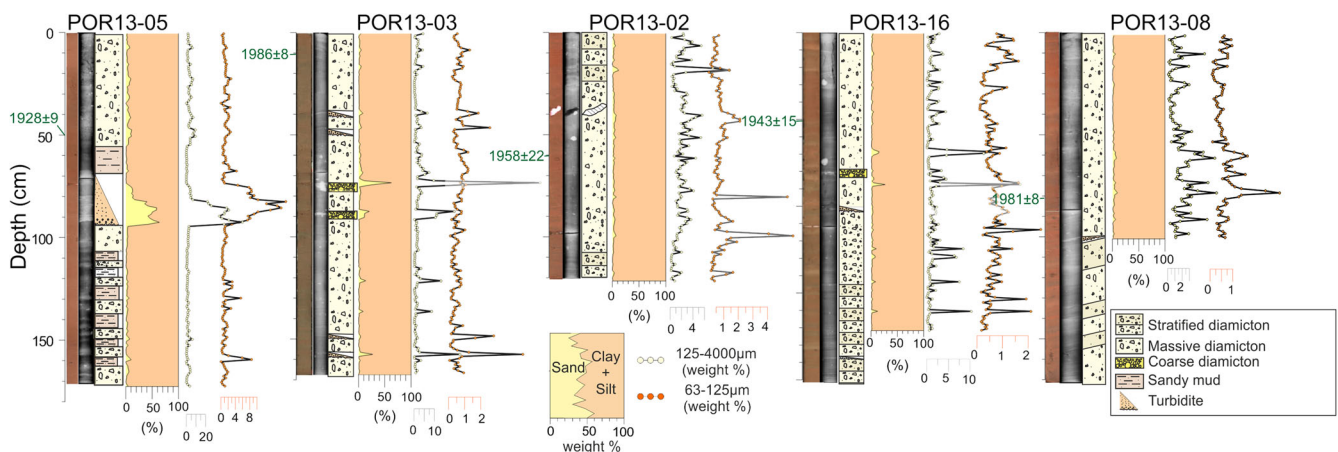


Figure 4. Overview of analysed cores and data analysis. From left to right: linescan, radiograph, lithology, grain-size distribution (sand vs clay +mud), wet-sieving results (63–125 and 125–4000 μm), together with age indications. Grain-size data available in Tables S2–S6. [Color figure can be viewed at wileyonlinelibrary.com]

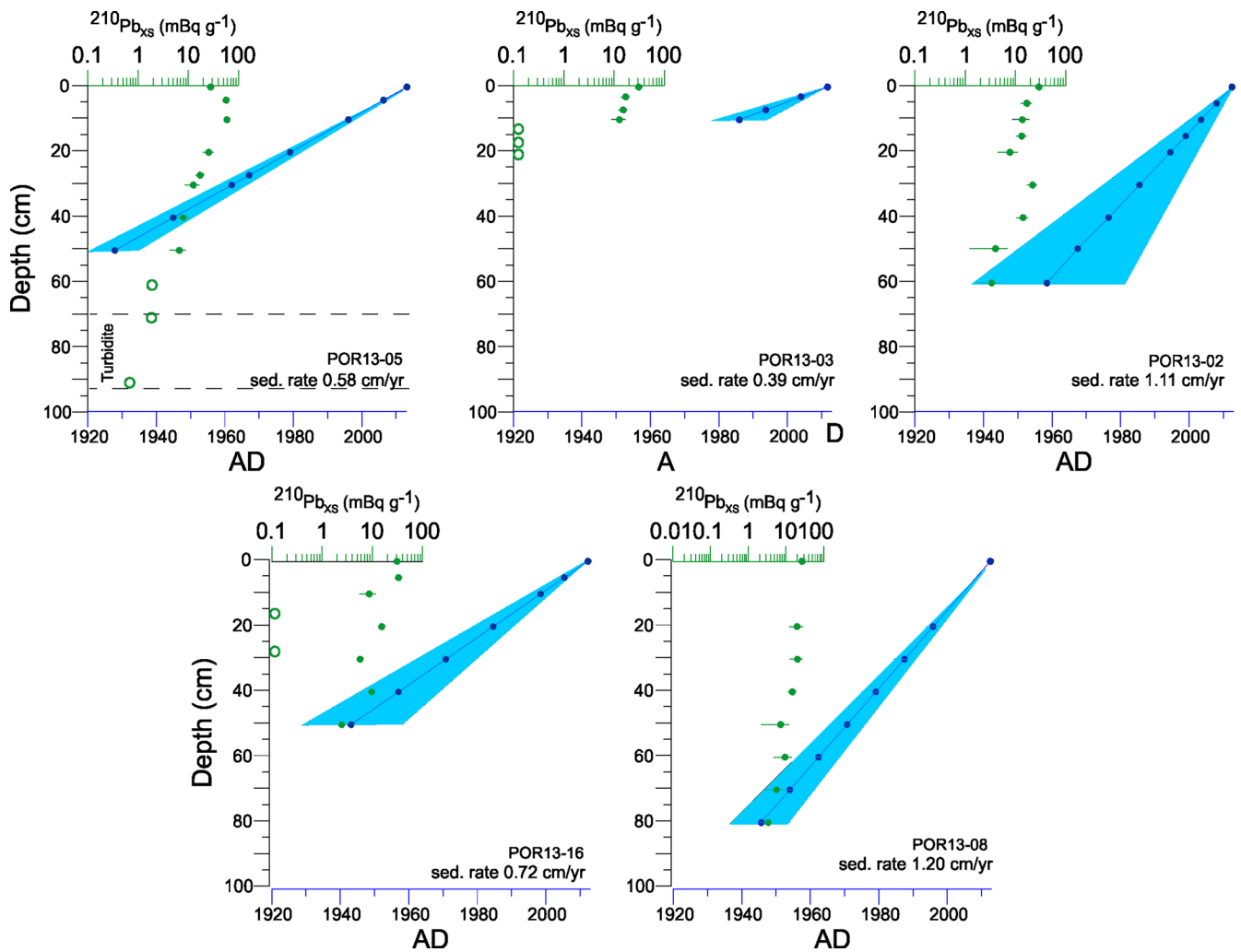


Figure 5. Profiles of $^{210}\text{Pb}_{\text{xs}}$ and corresponding age models. $^{210}\text{Pb}_{\text{xs}}$ values lower than 0.1 mBq g^{-1} are indicated as open circles and were not taken into account for calculating the age models (Table S7). [Color figure can be viewed at wileyonlinelibrary.com]

calving rates. It has been suggested that the IRD variations of multiple cores can be averaged in order to reduce the component and extract a signal that is more representative of the iceberg calving in the fjord (Andresen *et al.*, 2012). This approach leads to two questions: how many cores are required and which fjord locations should be sampled in order to obtain a representative signal? To test this we produce composites based on different combinations of the cores (Fig. S2). Core Fox 12-08 is not taken into account for these calculations since this core site only receives icebergs from Glacier 3 and 4, and is therefore not comparable with the other core sites, which receive icebergs from all 4 glaciers. The composite based on the four cores provides a relatively good agreement with the observed glacier changes (Fig. 8), but it should be taken into account that this signal is dependent of the amount of cores that are included (Fig. S2, data available in Table S8). Also, it is important to note that this correspondence is predominantly due to variability exhibited by core POR13-05, the outermost core site. This suggests that, in Upernavik Fjord, the outer fjord seems less prone to randomness related to ice-rafting. In Andresen *et al.*, (2012), cores in the middle of Sermilik Fjord were shown to provide the best correspondence to observed retreat. Therefore, in order to produce a reliable IRD record it may be more important to characterise IRD variability in the mid- to outer- fjord areas compared to the inner-fjord.

Another important conclusion of our comparison is that the amplitudes of the IRD peaks are not directly proportional to the rate of area change, and they are characterised by a generally

decreasing trend. This is particularly pronounced for the period of enhanced glacier retreat from 2003 to 2010 which is not well reflected in the IRD record (Fig. 8). The observed decrease in IRD flux with glacier margin retreat may be explained by the lengthening of iceberg transport pathways. As the distance between the calving front and the core site increases the sediment load of icebergs becomes progressively depleted which in turn reduces the amplitude of the IRD signal. This is supported by analysis of iceberg melt rates in Sermilik Fjord, showing a marked decrease in melting down fjord (Moon *et al.*, 2018). We anticipate that this pattern also occurs in Upernavik Isfjord. Therefore, our results imply that peaks in IRD fluxes (from the outer fjord) reflect periods of increased calving, but the relative sizing of IRD peak amplitudes is not directly proportional to the calving rate. Interpretations comparing calving rates derived from IRD amplitudes should thus take into account the potential influence from changes in the iceberg travel time and distance. This effect might be limited for sites further offshore (e.g. shelf/slope) because the relative change in distance is smaller for these sites.

Linking IRD variability, glacier retreat and climate in Upernavik Fjord

The glacier frontal position in 1886 aligns with a bathymetric high 125 m above the surrounding seafloor. The orientation and shape (Fig. 1) resemble the characteristics of a terminal

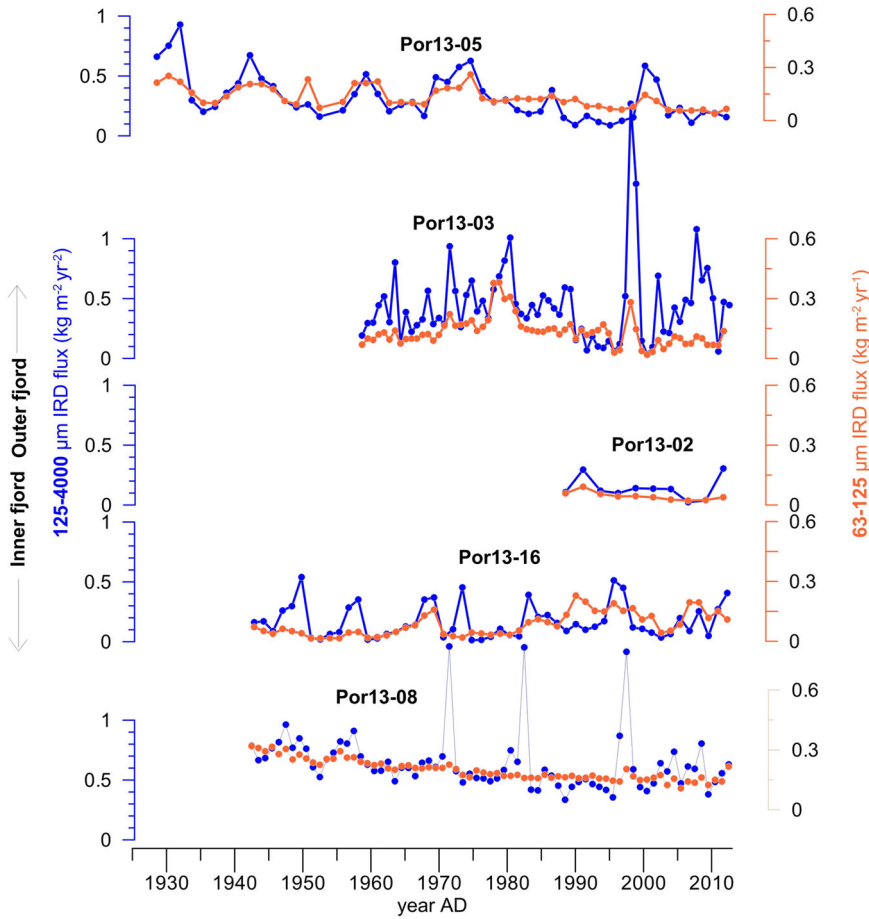


Figure 6. Comparison between 63–125 μm flux and 63–4000 μm flux for the different cores. [Color figure can be viewed at wileyonlinelibrary.com]

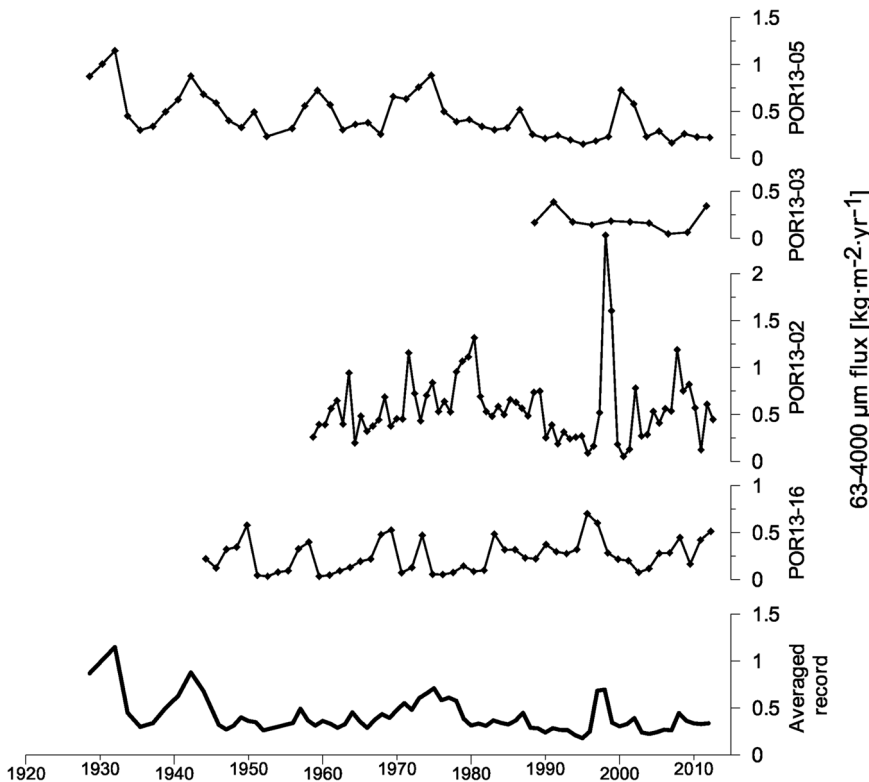


Figure 7. Variations in IRD fluxes (63–4000 micron) for the different cores plotted versus time, together with their average (data available in Table S8). POR13-08 was not incorporated into the average since this core site does not record icebergs from all four glaciers. Numbers in boxes the bottom of the figure refer to the amount of cores from which the average was calculated.

moraine and suggests that the ice margin remained stable at this location for a prolonged period of time. The inferred terminal moraine likely delineates the maximum extent of UI during the Little Ice Age. In the period between 1886 and 1931, UI retreated at a relatively slow pace. Accelerated glacier retreat commenced in 1931 and coincided with a

maximum of iceberg-rafting. Both retreat and calving further intensified in the 1940s. This period of glacier instability occurred during an episode of climatic warming in the entire Greenland region (Chylek *et al.*, 2006). Similar glacier instability in response to this warming has been reconstructed at Helheim Glacier (Andresen *et al.* 2012) and at Jakobshavn

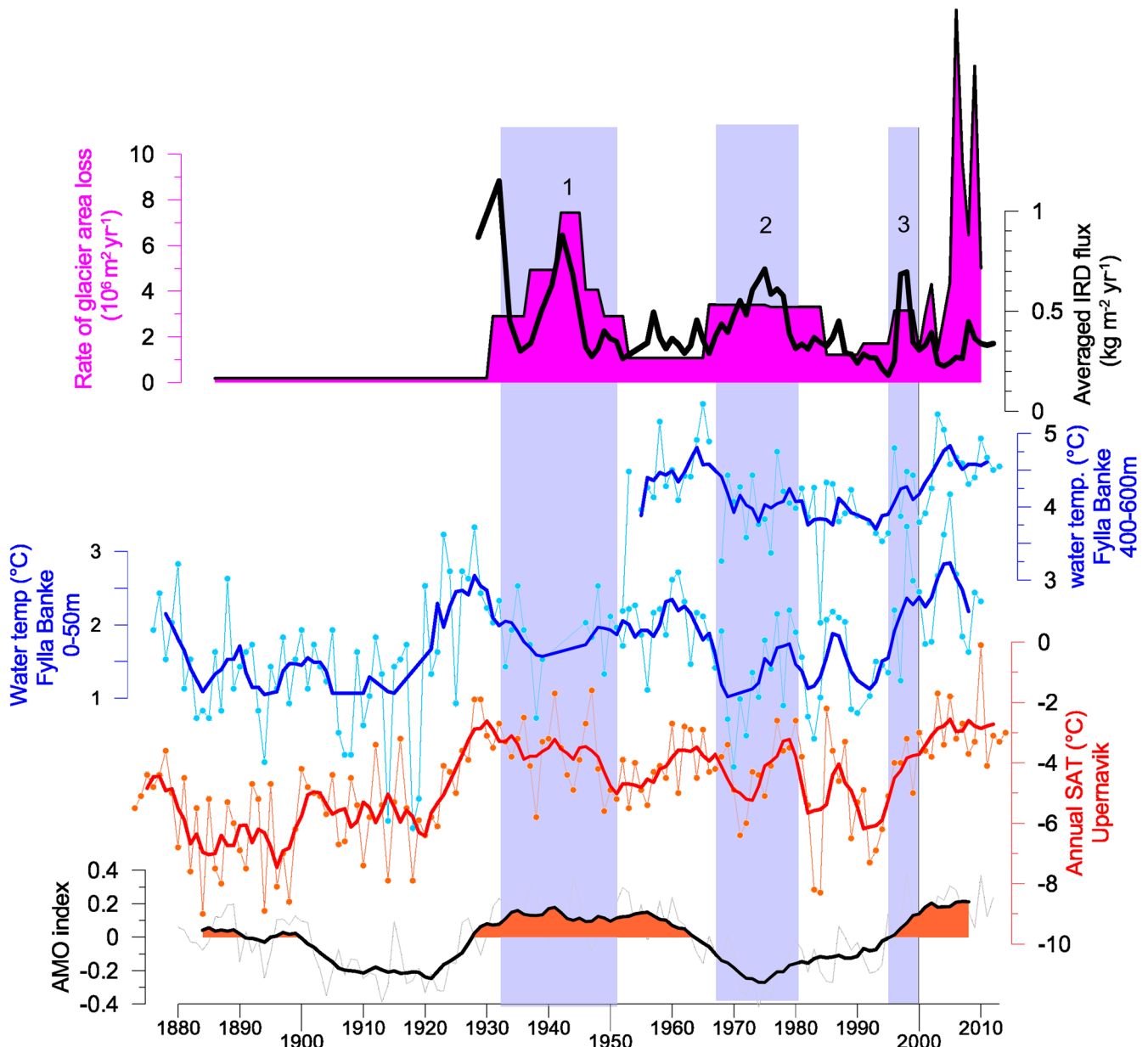


Figure 8. Comparison between the average IRD signal, glacier area change and regional climate. Shaded time intervals indicate the four periods with increased glacier area loss and IRD deposition. [Color figure can be viewed at wileyonlinelibrary.com]

Isbræ (Chylek *et al.*, 2006). This retreat phase of UI coincided with a positive phase of the Atlantic Multidecadal Oscillation (AMO); a climatic mode of variability expressed primarily in sea surface temperature in the wider North Atlantic Ocean (Schlesinger and Ramankutty, 1994; Faurshou *et al.*, 2011). The retreat of UI during this period was thus likely triggered by increased warming of subsurface ocean water and/or air temperatures.

A period of slower retreat occurred from the early 1950s to the mid '60s (Fig. 8). This was followed by increased icebergrafting and faster glacier retreat that lasted from the mid '60s until ~1980 and mid '80s, respectively. (Fig. 8). This retreat period is remarkable as it happened during a negative AMO phase. This was characterised by cold air and ocean temperatures in West Greenland, and other glaciers in the region were stabilising during this interval (Kjeldsen *et al.*, 2015; Rignot *et al.*, 2008). This episode of retreat may be attributable to the interplay between glacier dynamics and fjord geometry rather than an external forcing mechanism. Between 1976 and 1985, UI-4 retreated from the deep fjord basin (>700 m bsl) into shallower water with depths of <250 m

and continued to retreat steadily and asynchronously with the other three glaciers (Fig. 1 and 2A). UI-4 is thinner than its neighbouring glaciers and is therefore more sensitive to external forcing such as warming ocean and air temperatures (Oerlemans, 2008). Consequently, UI-4 reacts more rapidly to environmental changes, and retreat is further enhanced by its retrograde bed slope (Jamieson *et al.*, 2012). Thus, we propose that the retreat behaviour of UI-4 from 1970 was triggered by changes in ocean and air temperatures and this was then sustained by its bed topography.

The late 80's and early 90's were characterised by relatively low retreat rates and a low ice-rafting signal. A sharp increase in ice-rafting occurred between 1996 and 2000 and this corresponds with an increase in area loss at glaciers UI-1, UI-2, and UI-4 (Fig. 8). More specifically, the glacier front of UI-1 suddenly retreated 1 km after an 11 year period of relative stability (Khan *et al.*, 2013). UI-4 retreated 1 km during this period, and probably contributed to the relatively high peak in IRD. Kjær *et al.* (2012) and Khan *et al.* (2013) reported a dynamic thinning event that occurred between 1985 and 1994. The retreat of the glacier area and increased calving

signal that occurred after 1996 may be attributable to this event; it has been proposed that thinning of tidewater glaciers reduces basal resistance and increases sliding, which then leads to rapid calving and increased frontal retreat (Pritchard and Vaughan, 2007).

The increase in the rate of area loss that occurred between 2003 and 2010 is primarily due to the accelerated retreat of the northern glaciers (UI-1 and UI-2) (Khan *et al.*, 2013; Kjær *et al.*, 2012; Larsen *et al.*, 2016). Larsen *et al.* (2016) suggested that the retreat of UI-1 was triggered by warming of deeper ocean waters in the late 1990s. The IRD flux during this time period was surprisingly low, indicating minimal ice-rafting in the fjord (Fig. 8). It was already argued above that the increased travel distance of icebergs may reduce IRD deposition in the fjord. In addition to this, the low IRD signal during this period might be explained by the formation of a more stable ice mélange, which retains calved icebergs and thus confines IRD deposition to the mélange area (Syvitski *et al.*, 1996).

Conclusions

Using data from a transect of sediment cores, we show that the ice-rafting signal in Upernavik Isfjord over the past 90 years is characterised by a high spatial variability. We have used these results to investigate whether a better link between IRD records and glacier record can be established by averaging IRD records from multiple cores. The IRD composite based on four cores indeed corresponds relatively well to the record of glacier area change based on observations, but this is mostly due to the imprint on the average from a core located in the outer-fjord. In addition, we show that the comparison and interpretation of the amplitudes of IRD peaks should be done with caution since their relation to glacier retreat/calving is not linear and other processes may overprint the signal. This is for example reflected in the lack of an increased IRD signal in response to rapid retreat of the northern glaciers of Upernavik Isstrøm between 2003–2010.

We conclude that it is important that IRD reconstructions adequately investigate spatial variability and that, in the setting of a glacial fjord, targeting mid- to outer-fjord core sites might provide more reliable reconstructions compared to glacier proximal locations. Three periods of increased iceberg rafting were reconstructed for the 20th century: 1933–1946, 1968–1980, and 1996–1999. A comparison of these periods with climate records indicates that calving of Upernavik Isstrøm intensified in relation to warming temperatures in the late '30s/early '40s, late '90s, whereas increased iceberg productivity between 1968 and 1980 might be the result of a dynamic response to the geometry of the fjord.

Supporting Information

Additional supporting information can be found in the online version of this article.

Fig. S1. Measurements of ¹³⁷Cs compared to events known to have produced ¹³⁷Cs in atmosphere.

Fig. S2. Averaged composites of IRD flux based on each combination of three cores.

Table S1. Calculations of area changes of Upernavik Isstrøm since 1886, based on historical observations.

Table S2. Grain-size analysis of core POR13-02.

Table S3. Grain-size analysis of core POR13-03.

Table S4. Grain-size analysis of core POR13-05.

Table S5. Grain-size analysis of core POR13-08.

Table S6. Grain-size analysis of core POR13-16.

Table S7. Measurements of lead and caesium isotopes together with the age models of the sediment cores.

Table S8. Calculations of different averages of the IRD flux (63–4000 µm) based on different combinations of cores.

Acknowledgements. This study is a contribution to the VILLUM FONDEN project “Past and Future Dynamics of the Greenland Ice Sheet: what is the ocean hiding?” (10100). We thank the captain and crew of R/V Porsild. Christina Lyngø, Pernille Stockmarr and Glenn Oxfeldt Jensen are thanked for help with grain-size analysis. Sébastien Bertrand and an anonymous reviewer are thanked for insightful comments and suggestions relating to a previous version of the manuscript. We have no conflicts of interest to disclose.

References

- Andresen CS, Kjeldsen KK, Harden B *et al.* 2014. Outlet glacier dynamics and bathymetry at Upernavik Isstrøm and Upernavik Isfjord, North-West Greenland. *Geological Survey of Denmark and Greenland Bulletin* 79–82.
- Andresen CS, Straneo F, Ribergaard MH, 2011. Rapid response of Helheim Glacier in Greenland to climate variability over the past century. *Nature Geoscience* 5: 37–41.
- Andrews JT 2000. Icebergs and Iceberg Rafted Detritus (IRD) in the North Atlantic: Facts and Assumptions. *Oceanography* 13: 100–108.
- Appleby PG 2008. Three decades of dating recent sediments by fallout radionuclides: a review. *The Holocene* 18: 83–93. <https://doi.org/10.1177/0959683607085598>
- Bouma AH 1962. *Sedimentology of some Flysch deposits: A graphic approach to facies interpretation*. Elsevier B.V.
- van den Broeke MR, Enderlin EM, Howat IM *et al.* 2016. On the recent contribution of the Greenland ice sheet to sea level change. *Cryosphere* 10: 1933–1946. <https://doi.org/10.5194/tc-10-1933-2016>
- Chylek P, Dubey MK, Lesins G 2006. Greenland warming of 1920–1930 and 1995–2005. *Geophysical Research Letters* 33: 1–5. <https://doi.org/10.1029/2006GL026510>
- Dowdeswell JA, Whittington RJ, Marienfeld P 1994. The origin of massive diamicton facies by iceberg rafting and scouring, Scoresby Sund, East Greenland. *Sedimentology* 41: 21–35.
- Escher JC, Pulvertaft TCR 1995. Geological map of Greenland. Geological Survey of Greenland: Copenhagen. 1: 2 500 000
- Fenty I, Willis J, Khazendar A *et al.* 2016. Oceans Melting Greenland: Early Results from NASA's Ocean-Ice Mission in Greenland. *Oceanography* 29: 72–83.
- Haubner K, Box JE, Schlegel NJ *et al.* 2017. Simulating ice thickness and velocity evolution of Upernavik Isstrøm 1849–2012 by forcing prescribed terminus positions in ISSM. *The Cryosphere Discussions* 1–16. <https://doi.org/10.5194/tc-2017-121>
- Heinrich H 1988. Origin and consequences of cyclic ice rafting in the Northeast Atlantic Ocean during the past 130,000 years. *Quaternary Research* 29: 142–152.
- Jamieson SSR, Vieli A, Livingstone SJ *et al.* 2012. Ice-stream stability on a reverse bed slope. *Nature Geoscience* 5: 799–802.
- Khan SA, Kjær KH, Korsgaard NJ *et al.* 2013. Recurring dynamically induced thinning during 1985 to 2010 on Upernavik Isstrøm, West Greenland. *Journal of Geophysical Research: Earth Surface* 118: 111–121. <https://doi.org/10.1029/2012JF002481>
- Kjeldsen KK, Korsgaard NJ, Bjørk AA *et al.* 2015. Spatial and temporal distribution of mass loss from the Greenland Ice Sheet since AD 1900. *Nature* 528: 396–400. <https://doi.org/10.1038/nature16183>
- Kjær KH, Khan SA, Korsgaard NJ *et al.* 2012. Aerial Photographs Reveal Late-20th-Century Dynamic Ice Loss in Northwestern Greenland. *Science* 337: 569–573. <https://doi.org/10.1126/science.1220614>
- Klouch KZ, Schmidt S, Andrieux-Loyer F *et al.* 2016. Historical records from dated sediment cores reveal the multidecadal dynamic of the toxic dinoflagellate *Alexandrium minutum* in the Bay of Brest (France). *FEMS Microbiology Ecology* 92: 1–16. <https://doi.org/10.1093/femsec/fiw101>

- Kuijpers A, Knutz P, Moros M (2014) Ice-Rafted Debris, *Encyclopedia of Marine Geosciences*, J Harff, M Meschede, S Petersen, & J Thiede eds., Springer Science+Business Media: Dordrecht. pp. 1–7. <https://doi.org/10.1007/978-94-007-6644-0>
- Larsen SH, Khan SA, Ahlstrøm AP *et al.* 2016. Increased mass loss and asynchronous behavior of marine-terminating outlet glaciers at Upernavik Isstrøm, NW Greenland. *Journal of Geophysical Research F: Earth Surface* **121**: 241–256. <https://doi.org/10.1002/2015JF003507>
- MacKenzie AB, Hardie SML, Farmer JG *et al.* 2011. Analytical and sampling constraints in ²¹⁰Pb dating. *Science of the Total Environment* **409**: 1298–1304. <https://doi.org/10.1016/j.scitotenv.2010.11.040>
- Meischner D, Rumohr J 1974. A light-weight, high-momentum gravity corer for subaqueous sediments. *Senckenbergiana maritima* **6**: 105–117.
- Moon T, Sutherland DA, Carroll D *et al.* 2018. Subsurface iceberg melt key to Greenland fjord freshwater budget. *Nature Geoscience* **11**: 49–54. <https://doi.org/10.1038/s41561-017-0018-z>
- Ó Cofaigh C, Dowdeswell JA 2001. Laminated sediments in glacial marine environments: Diagnostic criteria for their interpretation. *Quaternary Science Reviews* **20**: 1411–1436.
- Pritchard HD, Vaughan DG 2007. Widespread acceleration of tide-water glaciers on the Antarctic Peninsula. *Journal of Geophysical Research: Earth Surface* **112**: 1–10. <https://doi.org/10.1029/2006JF000597>
- Ribergaard MH, Olsen SM, Mortensen J 2008. *Oceanographic Investigations off West Greenland 2007*. Danish Meteorological Institute Centre for Ocean and Ice.
- Rignot E, Box JE, Burgess E *et al.* 2008. Mass balance of the Greenland ice sheet from 1958 to 2007. *Geophysical Research Letters* **35**: 1–5. <https://doi.org/10.1029/2008GL035417>
- Straneo F, Heimbach P 2013. North Atlantic warming and the retreat of Greenland's outlet glaciers. *Nature* **504**: 36–43.
- Syvitski JPM, Andrews JT, Dowdeswell JA 1996. Sediment deposition in an iceberg-dominated glacial marine environment, *Global and Planetary Change*. basin fill implications: East Greenland. 251–270. [https://doi.org/10.1016/0921-8181\(95\)00023-2](https://doi.org/10.1016/0921-8181(95)00023-2)
- Wangner DJ, Jennings AE, Vermassen F *et al.* 2018. A 2000-year record of ocean influence on Jakobshavn Isbræ calving activity, based on marine sediment cores. *The Holocene* **28**: 1731–1744. <https://doi.org/10.1177/0959683618788701>
- Weidick A 1958. Frontal Variations at Upernaviks Isstrøm in the Last 100 Years. *Meddelser fra Dansk Geologisk Forening København* **14**: 52–60.